Explaining the Spatial Pattern of U.S. Extreme Daily Precipitation Change

MARTIN HOERLING[a], LESLEY SMITH,[a,b] XIAO-WEI QUAN,[a,b] JON EISCHEID,[a,b] JOSEPH BARSUGLI,[a,b] AND HENRY F. DIAZ[c]

[a] *NOAA/Physical Sciences Laboratory, Boulder, Colorado*
[b] *University of Colorado, Cooperative Institute for Research in Environmental Sciences, Boulder, Colorado*
[c] *University of Hawai'i at Mānoa, Honolulu, Hawaii*

(Manuscript received 25 August 2020, in final form 21 December 2020)

ABSTRACT: Observed United States trends in the annual maximum 1-day precipitation (RX1day) over the last century consist of 15%–25% increases over the eastern United States (East) and 10% decreases over the far western United States (West). This heterogeneous trend pattern departs from comparatively uniform observed increases in precipitable water over the contiguous United States. Here we use an event attribution framework involving parallel sets of global atmospheric model experiments with and without climate change drivers to explain this spatially diverse pattern of extreme daily precipitation trends. We find that RX1day events in our model ensembles respond to observed historical climate change forcing differently across the United States with 5%–10% intensity increases over the East but no appreciable change over the West. This spatially diverse forced signal is broadly similar among three models used, and is positively correlated with the observed trend pattern. Our analysis of model and observations indicates the lack of appreciable RX1day signals over the West is likely due to dynamical effects of climate change forcing—via a wintertime atmospheric circulation anomaly that suppresses vertical motion over the West—largely cancelling thermodynamic effects of increased water vapor availability. The large magnitude of eastern U.S. RX1day increases is unlikely a symptom of a regional heightened sensitivity to climate change forcing. Instead, our ensemble simulations reveal considerable variability in RX1day trend magnitudes arising from internal atmospheric processes alone, and we argue that the remarkable observed increases over the East has most likely resulted from a superposition of strong internal variability with a moderate climate change signal. Implications for future changes in U.S. extreme daily precipitation are discussed.

KEYWORDS: Climate records; Climate models; Climate change; Extreme events; Precipitation

1. Introduction

The intensity of extreme daily precipitation has increased over the contiguous United States. A nationally averaged upward trend is robust across analyses spanning different historical periods, for example commencing at the beginning of the twentieth century (Karl and Knight 1998; Westra et al. 2013), emerging from the 1930s' Dust Bowl era (Kunkel et al. 1999), and also since the 1950s (Dittus et al. 2015). The observed increase at this continental scale is attributable in part to human-induced climate change (Min et al. 2011; Dittus et al. 2016; Paik et al. 2020; Kirchmeier-Young and Zhang 2020) consistent with the physical link between rising greenhouse gas concentrations, global warming, atmospheric moistening, and the constraint that water vapor exerts on extreme precipitation intensity (e.g., Trenberth 1999; Allen and Ingram 2002; Allan and Soden 2008; O'Gorman and Schneider 2009).

The U.S. trend is part of a larger-scale pattern of heavy precipitation increase that has been observed across middle and higher latitudes. Model simulations reveal a dominant thermodynamic effect of climate change over those regions whose trend magnitudes scale approximately with the Clausius–Clapeyron (C-C) rate of 7% $°C^{-1}$ (Emori and Brown 2005; Pall et al. 2007; Fischer and Knutti 2016). Dynamic contributions of climate change to extreme precipitation, as inferred from changes in tropospheric vertical velocities, can modify this otherwise spatially homogeneous thermodynamic contribution. However, analysis based on climate model simulations of phase 5 of the Coupled Model Intercomparison Project (CMIP5) indicate that significant dynamical effects appear to be confined to the tropics and the Mediterranean region. As such, a rather homogeneous increase in extreme daily precipitation is generally expected to arise in the midlatitudes due to a mostly spatially invariant increase in moisture availability (Pfahl et al. 2017).

Yet, the regional pattern of observed heavy precipitation trends across the United States departs from this theoretical expectation, being remarkable for its heterogeneity rather than the more uniform structure that thermodynamic effects alone would predict. Recent assessments have emphasized the strong increases over the U.S. Northeast and Midwest where percent changes since the early twentieth century have far exceeded a rate suggested by C-C scaling (Easterling et al. 2017; USGCRP 2018). By contrast, the U.S. Southwest has exhibited declines in heavy precipitation intensity.

The regionally diverse trends in extreme precipitation are likely related to dynamical factors. Over the Northeast, upward trends in both extratropical cyclone-related and tropical cyclone-related extreme precipitation have been observed during 1908–2009, whereas a downward trend in extratropical

Supplemental information related to this paper is available at the Journals Online website: https://doi.org/10.1175/JCLI-D-20-0666.s1.

Corresponding author: Dr. Martin Hoerling, martin.hoerling@noaa.gov

DOI: 10.1175/JCLI-D-20-0666.1

cyclone-related extremes has occurred in the U.S. Southwest (Barlow 2011; Kunkel et al. 2012). The Southwest decline in heavy precipitation events has been further linked to dynamics of atmospheric teleconnections in response to decadal variations in tropical Pacific sea surface temperature (SST; Hoerling et al. 2016). The extent to which such regionally diverse dynamical mechanisms for heavy precipitation change may reflect long-term climate change effects is, however, not currently known. Assessment reports to date have emphasized the current understanding of observed trends for *national averages* of heavy precipitation, arguing those to be explainable by well-established physical constraints and expectations in a warming world (Easterling et al. 2017; USGCRP 2018). But the nature of the *diverseness in regional trends* in heavy precipitation changes across the contiguous United States does not align with a simple thermodynamic argument, motivating research into its possible dynamical origins.

It is generally agreed that multidecadal variability can dictate the characteristics of trends at local-to-regional scales (Deser et al. 2014; Fischer and Knutti 2014; Hoerling et al. 2016; Fischer et al. 2014). As such—and perhaps this recognition informs a prevailing view—the spatial heterogeneity in U.S. heavy precipitation trends is plausibly suspected to reflect internal variability. If true, one should expect a slowing in the rate of heavy precipitation rise in the Northeast and a reversal in the downward trend in the Southwest, thereby tending to a more uniform spatial pattern expected from thermodynamics of climate change. But such suppositions must first be placed on firmer grounds that include diagnosing both thermodynamic and dynamic effects of climate change and comparing the resulting overall signal of forced change to the trend patterns that can arise from purely naturally occurring internal variations.

In this study, we explore the causes for the spatially heterogeneous pattern of U.S. extreme precipitation change observed over the last century. Our focus keys on the question whether such a pattern could be a manifestation of anthropogenic climate change. Our approach builds on prior studies that stress the importance of using large multimember ensembles of model runs—and also the use of multiple models—for robustly identifying forced signals of extreme precipitation change regionally (e.g., Fischer et al. 2014). Also, recognizing the importance of horizontal resolution on the quality of simulated extreme precipitation, this study employs global models conducted at a nominal 50-km resolution, which has been deemed a "breakthrough" resolution (Wehner et al. 2010, 2014; van der Wiel et al. 2016) for achieving realistic magnitudes of annual maximum daily precipitation intensity compared to 100- and 200-km spatial resolutions employed in most CMIP3 and CMIP5 models and many CMIP6 models.

The experimental approach applies an event attribution framework that has been used previously to assess climate change effects on individual extreme events (National Academy of Sciences Engineering and Medicine 2016), and also in explaining long-term trends at regional scales [see Hoerling et al. (2019) and references therein]. Parallel sets of atmospheric model simulations are conducted, one in which the ocean surface and sea ice boundary condition and atmospheric chemical composition are prescribed to vary as observed under recent climate conditions of the early twenty-first century (*factual simulation*) and the other which experiences nearly identical interannual and decadal variations as if such variations had occurred under climate conditions at the turn of the twentieth century (*counterfactual simulation*). The method of running pairs of atmospheric models—one including all forcings and the other only natural forcings (including an estimate of internal boundary conditions)—is the backbone of event attribution systems used in the broader community (e.g., Christidis et al. 2013; Massey et al. 2015; Ciavarella et al. 2018). Each of these systems is based primarily on a single atmospheric modeling system, uses very large ensembles, and employs high horizontal resolution (e.g., the Wx@Home approach of Massey et al. is performed at ~40-km resolution, and the Hadley Center attribution system of Ciavarella et al. at ~60 km in the midlatitudes). Our analysis is conducted at similar spatial scales and utilizes three different atmospheric models to further probe robustness to structural model uncertainty. We focus on the comparison of extreme precipitation statistics between such pair of simulations, thereby contrasting their characteristics in the current warm world to that in an appreciably colder world of about a century earlier.

Section 2 describes the models and methods used herein in detail. The quality of daily rainfall in the models compared to observations over the contiguous United States is evaluated in section 3. The principal metric of extreme precipitation to be studied herein is the annual maximum 1-day precipitation (RX1day), for which simulations of both its climatological intensity and seasonal cycle are first evaluated. Results on climate change sensitivity of RX1day are presented in section 4. Using a non-fingerprint-based detection and attribution method that focuses on pattern-based agreement of observed and modeled changes, (e.g., van Oldenborgh et al. 2013; Knutson et al. 2013; Wuebbles et al. 2017) the observed pattern of RX1day change is interpreted in the context of a pattern attributable to climate change and a pattern due to internal variability. Section 4 interprets the forced pattern of RX1day in both a thermodynamic and dynamic context, the former inferred from the relationship between simulated RX1day and precipitable water change and the latter inferred from forced signals of large-scale atmospheric circulation changes. A summary and concluding remarks appear in section 5.

2. Datasets and model experiments

a. Observations

Precipitation data are from the gauge-based daily gridded Climate Prediction Center (CPC) Unified analysis (Xie et al. 2007). These are based on approximately 8000 observation locations over the contiguous United States from multiple sources including the Global Telecommunication System (GTS), Cooperative observers (COOP), and other national agencies (Chen et al. 2008). The daily data are gridded at 0.25°, and the period of analysis is 1948–2018.

The study also uses a 1° gridded daily precipitation dataset for 1901–2018 that is based on the Global Historical Climate

TABLE 1. Atmospheric model description.

Model	Resolution	Vertical levels	Cumulus parameterization	Ensemble
CAM5	0.45° × 0.6° (~50 km)	30 levels 2 hPa top	Zhang–McFarlane	18
ECHAM5	T157 (nominal 75 km)	31 levels 10 hPa top	Tiedtke	50
MRI-3.2	T319 (nominal 60 km)	64 levels 0.01 hPa top	Arakawa–Schubert	25

Network of daily station records (GHCN-D), though having sparser availability in early decades (Menne et al. 2012).

For the same 70-yr historical period, reanalysis products of total column precipitable water (PW) and tropospheric geopotential heights are analyzed to describe thermodynamic and dynamic changes accompanying heavy precipitation change. The data sources are NCEP–NCAR reanalysis (Kalnay et al. 1996), the Twentieth Century Reanalysis, version 3 (20th CRv3; Compo et al. 2011), and the JRA-55 product (Kobayashi et al. 2015). The NCEP–NCAR data span the entire 1948–2018 period, the 20th CRv3 used herein spans 1948–2015, and JRA-55 covers 1958–2018.

b. *Climate models and experiments*

Three global atmospheric models (Table 1) are used, which are identical to those studied previously in Hoerling et al. (2019): the National Center for Atmospheric Research Community Atmospheric Model (CAM5; Neale et al. 2012), the European Centre for Medium-Range Weather Forecasts/Hamburg model (ECHAM5; Roeckner et al. 2003), and Japan's Meteorological Research Institute model (MRI3.2; Mizuta et al. 2017). Each model represents horizontal scales in middle latitudes of ~50 km. The model variables examined are RX1day (derived from statistics of daily precipitation), PW, 700-hPa geopotential heights, and 500-hPa vertical velocity. For brevity, the models are subsequently referred to as CAM, ECHAM, and MRI. The authors performed the CAM and ECHAM model runs, while the MRI runs were performed by the Japanese Meteorological Research Institute.

Pairs of atmospheric simulations are conducted for each model. One, referred to as the factual experiment, simulates climate near the turn of the twenty-first century subjected to specified recent observed boundary conditions and atmospheric chemical composition. Monthly SST and sea ice concentration variations are based on Hurrell et al. (2008) in CAM and ECHAM, and on the Centennial In Situ Observation-Based Estimates of the Variability of SST and Marine Meteorological Variables, version 2 (COBE-2; Hirahara et al. 2014), in MRI. Greenhouse gases (GHGs), aerosol, and ozone variability in CAM and MRI use the protocol of CMIP5 historical forcings for 1901 through 2005 (see Neale et al. 2012; Mizuta et al. 2017). For ECHAM, GHGs vary according to the observed concentrations (Meinshausen et al. 2011), while tropospheric and stratospheric ozone vary based on Cionni et al. (2011). Aerosol concentrations do not vary interannually in ECHAM nor do they undergo any long-term trends. Long-term aerosols trends, which are believed to play a role in extreme precipitation trends, are not included in the ECHAM experiments (e.g., Lin et al. 2016; Mascioli et al. 2016).

The CAM and ECHAM extensions after 2005 assume RCP6.0 forcing, while MRI assumes RCP8.5 forcing. The period of these historical runs is January 1979–December 2018 for CAM and ECHAM, and 1950–2010 for MRI.

The counterfactual experiments simulate climate near the turn of the twentieth century in which the boundary conditions and atmospheric composition are specified as if global warming had not occurred. The procedures follow those used in extreme event attribution studies (e.g., Pall et al. 2011; Stott et al. 2013; Christidis et al. 2013; Massey et al. 2015; Sun et al. 2018), and the specific methods applied to the current suite of simulations are described in Hoerling et al. (2019). The experiments are based on atmospheric models that are forced with monthly varying boundary conditions that retain the interannual and decadal variability of present-day climate occurring in the factual simulation but in which estimates of long-term ocean warming have been removed. Additionally, the GHG and ozone concentrations are set to turn of the twentieth-century values.

Concerning ocean boundary conditions, counterfactual SSTs are generated by removing an observed annual linear SST trend from the full variability. Detection of the anthropogenic component of long-term trends has, to date, been most robust for large spatial averages such as zonal means, whereas some regional patterns may be more significantly impacted by internal decadal variability (Knutson et al. 2013). Here, two different techniques are used in constructing the "pre–global warming" ocean boundary states; details of the model configurations and counterfactual development for CAM and ECHAM are provided in Sun et al. (2018), and those for MRI are in Mizuta et al. (2017). Only zonally averaged values of the trends are removed in CAM and ECHAM for the period 1880–2011. For MRI, a similar approach is used in that the SST warming pattern is also derived from observations except that the baseline for detrending is the beginning of the twentieth century, and trends at each grid point are removed rather than zonal averages. These two SST warming patterns are shown in Fig. 1 (left panels). All zonally averaged latitude bands exhibit warming having largest magnitudes of 0.6°–0.8°C in the tropics and Southern Ocean (top). The regional structure of the observed SST trends is characterized by greater warming in the Indian Ocean and tropical western Pacific relative to the tropical eastern Pacific (bottom; see also Solomon and Newman 2012). For comparison to these observed SST change patterns, Fig. 1 (right) shows SST trends from a 22-model average of CMIP6 historical simulations. The general agreement in magnitudes of

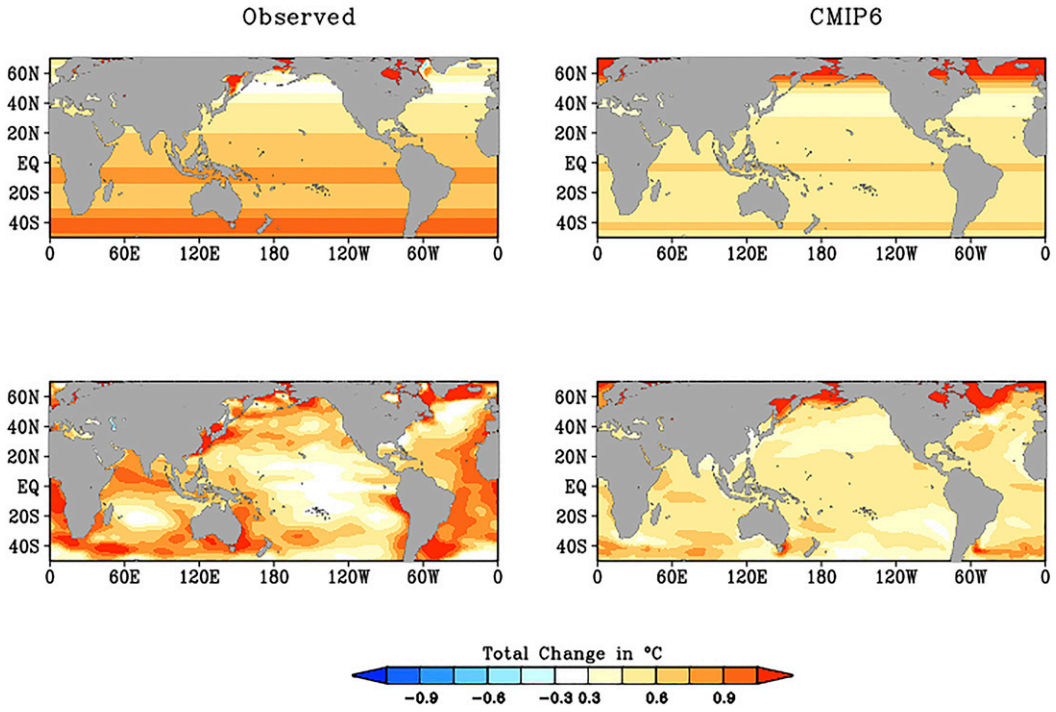

FIG. 1. (left) Observed SST trends (total change; °C) used in the construction of counterfactual SST boundary conditions for (top) CAM and ECHAM and (bottom) MRI model experiments. The former are based on ERSSTv3 analyses and the latter on COBEv2 analyses. (right) Simulated SST trends in CMIP6 historical experiments based on an average of 22 models. The zonally averaged trend patterns in top panels are for 1880–2011. The two-dimensional trend patterns in bottom panels are for 1900–2011.

observed ocean warming and the ensemble simulated changes occurring in response to external radiative forcing suggest that the former can be broadly understood as resulting from human-induced climate change. A formal attribution of the observed SST trends is not conducted, however, and we recognize that some features of the observed changes likely include manifestations of internal coupled ocean–atmosphere variability. The responses in factual versus counterfactual experiments are therefore strictly indicative of sensitivity to observed changes in boundary forcings over roughly the last century, and not necessarily due to anthropogenic climate change forcing alone. Our intercomparison of results from CAM and ECHAM models with the MRI model—which does include the full-field SST trends—permits study of robustness of RX1day sensitivity among experiments that include and exclude the possible effects of changes in east–west SST gradients (see Fig. 1).

A potential strength of using AMIP methods versus a CMIP approach is that the former is subjected to observed SSTs and their variations, thereby removing effects of the large SST biases that exist in coupled models. Some prior event attribution methods with atmospheric models have included CMIP SST trends as a way to estimate the climate change signal in ocean boundary conditions, together with observed trends (e.g., Christidis et al. 2013; Massey et al. 2015). The different methods of framing attribution based on coupled versus atmospheric models is discussed by Christidis et al. (2018), who noted that the largest uncertainty in their analysis of climate change impacts on the U.K. warm/wet winter of 2015/16 arose from assumptions about the SST change pattern. Here we have used only long-term SST trends based on observations. It remains an open question as to the best approach for determining the pattern of global SST warming, and thus the best procedure for counterfactual construction. Our study employs two different approaches for generating such global warming patterns and those provide some measure of uncertainty to the counterfactual design.

c. *Diagnosing climate change impacts on RX1day*

For each model, and for both factual and counterfactual experiments, an ensemble of simulations is generated whereby each member of a particular model experiences identical time evolving boundary forcing but initialized from different atmospheric initial states. In this study, 18, 50, and 25 members of the CAM, ECHAM, and MRI model, respectively, are analyzed.

For the recent 20-yr period 1999–2018, we calculate the factual minus counterfactual differences of RX1day, PW, and geopotential heights to quantify the effects of changes in climate drivers that have taken place over roughly the last century. For the MRI model whose simulations end in 2010, we use the 20-yr period of 1991–2010. We have verified, from the CAM and ECHAM data, that the simulated climate sensitivities are not materially different between contrasting the paired experiments for 1999–2018 versus 1991–2010 (not shown). The model sensitivities to climate change are compared with observed trends,

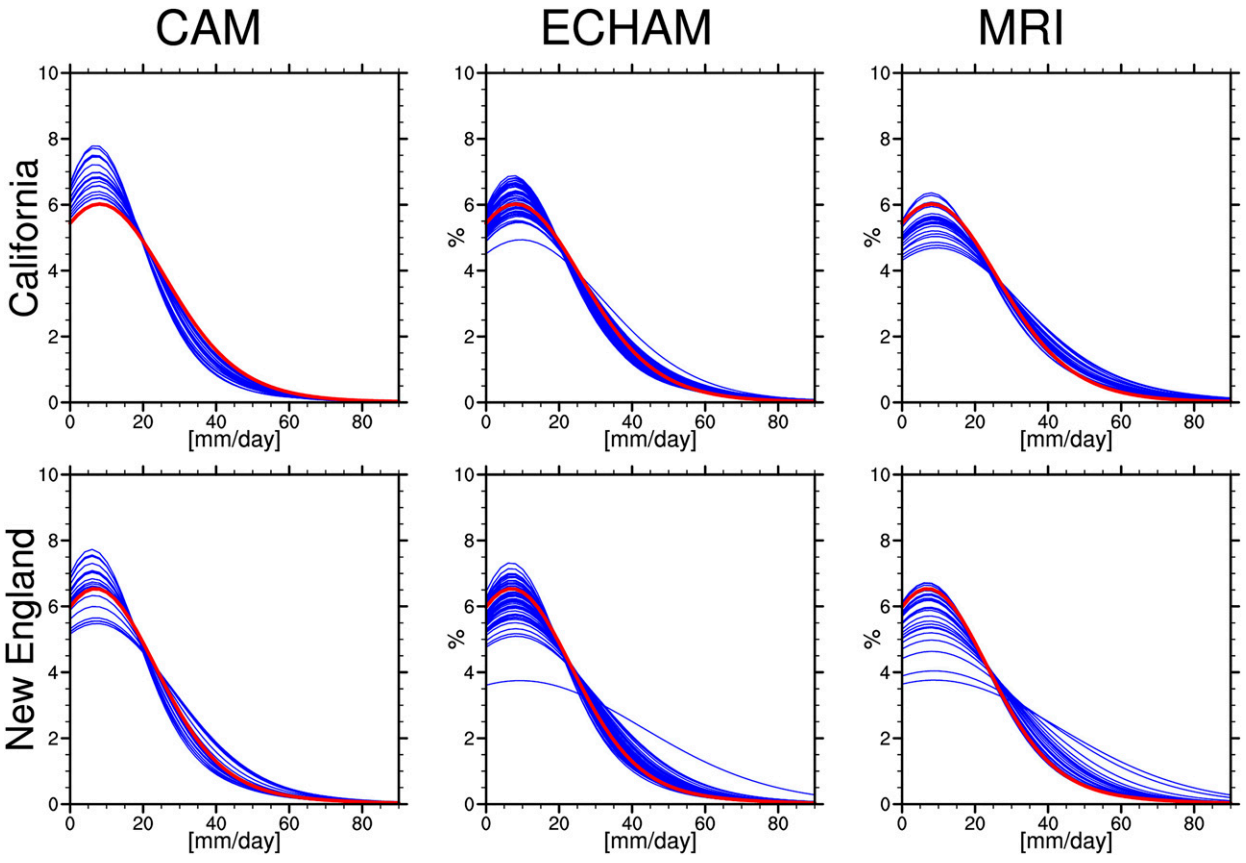

FIG. 2. Histograms of daily precipitation (mm day^{-1}) for a grid box in (top) central California near San Francisco and (bottom) coastal New England near Boston. Observations (red curve) are based on 1948–2018 CPC gridded daily analysis, model (blue curves) based on individual members of historical AMIP simulations for 1979–2018 based on (left) CAM and (center) ECHAM, and for 1979–2010 based on (right) MRI. All precipitation days exceeding 1 mm day^{-1} are included. The probability distribution functions are nonparametric curves constructed using the R software program, which utilizes a kernel density estimation and a Gaussian smoother.

calculated from 1999–2018 minus 1948–67 differences. We find that the observed RX1day changes are qualitatively similar when calculated from a smaller set of available stations that extend to 1901, and thus the post-1948 change highlighted herein is representative of a longer-term change pattern (see Fig. S1 in the online supplemental material).

The ensemble and paired modeling approach permit construction of a large sample of centennial-scale changes. Because ensemble members are effectively independent samples of atmospheric variability, any combination of factual and counterfactual simulation could occur with equal likelihood. For CAM, a total of 324 (18×18) unique centennial differences are generated, whereas a total of 2500 (50×50) and 625 (25×25) differences are calculated for ECHAM and MRI, respectively, where the numbers in parentheses denote the number of factual and counterfactual experiments. The forced component of change (i.e., the signal) is derived from the ensemble mean of differences, while the internal component (i.e., the noise due solely to atmospheric sampling variability) is estimated from the spread among ensemble members. We apply a simple detection and attribution approach to explaining the character of observed RX1day changes over the last century. The observed changes, in particular the U.S. pattern of RX1day changes, are compared with the statistics of simulated changes to determine the extent to which the former is consistent with variability that includes or excludes climate change drivers. This approach is referred to as a non-fingerprint-based approach to detection and attribution (Wuebbles et al. 2017), and we note that our signal detection is computed with respect to atmospheric variability alone, with the oceanic (SST and sea ice) differences being the same in each run, thus underestimating the true natural variability.

3. Climatological daily precipitation in observations and models

Smoothed histograms [nonparametric probability density functions (PDFs)] of climatological daily precipitation are shown for two selected grid points, one in vicinity of San Francisco, California (Fig. 2, top), and the other near Boston, Massachusetts (Fig. 2, bottom), as an illustration of model capabilities and biases. These two regions are selected for analysis because they anchor locations having very different observed trends in extreme daily precipitation as will be shown

TABLE 2. Climatological thresholds for observed and model extreme daily precipitation (mm).

	95th percentile	99th percentile	99.9th percentile
California			
OBS	33.0	50.5	92.5
CAM	32.9 ± 1.5	54.4 ± 2.9	85.7 ± 10.1
ECHAM	39.7 ± 1.8	64.4 ± 3.2	95.8 ± 9.3
MRI	42.0 ± 2.0	71.2 ± 3.8	111.0 ± 11.0
New England			
OBS	31.0	55.7	88.7
CAM	33.9 ± 1.1	57.5 ± 2.3	90.6 ± 8.0
ECHAM	34.6 ± 1.0	58.3 ± 2.5	94.1 ± 7.9
MRI	32.8 ± 0.8	55.7 ± 1.8	96.5 ± 9.2

in section 4. For each model, the PDFs are displayed for the ensemble of present-day (factual) climate simulations (blue curves). These are superposed on the CPC Unified gridded estimate of observations (red curve). For the central California location, CAM underestimates heavy precipitation events with a notable excess of light daily rain events, even when accounting for sampling uncertainty among ensemble members. By contrast, MRI overestimates the frequency of heavy events, whereas the ECHAM histograms most closely capture the behavior seen in observations across the range from light to heavy rain days. That is, the observed distribution is a more likely occurrence in the ECHAM ensemble, whereas it is at or near the extremes of the other two model ensembles. The CAM and ECHAM models are somewhat in better agreement with each other and with observations in the Northeast.

Table 2 summarizes the magnitudes of climatological daily totals for various conventional extreme thresholds. In observations, both locations experience very similar magnitudes for their 95th-, 99th-, and 99.9th-percentile daily event, roughly 30, 50, and 90 mm, respectively. These are compared to the average thresholds for each of the models, including the standard deviation among ensemble members that indicates the sampling variability for these various extreme event magnitudes. For both locations, the model threshold magnitudes tend to exceed the observed threshold. Note that since the observed data used here are grid averages, it is expected that individual stations would experience somewhat greater threshold magnitudes. Nonetheless, when compared to collocated model grids, this spatial average of the observed regional climatology including its quantitative character is well captured in CAM and ECHAM simulations within the sampling uncertainty. MRI in contrast significantly exceeds the observed extreme event magnitudes for rainfall in vicinity of San Francisco, even when accounting for sampling variability, although it is more closely aligned with observations for rainfall extremes in the vicinity of Boston.

The spatial distribution of the magnitude for the climatological wettest day of the year (RX1day) in shown in Fig. 3 (right) for the entire contiguous United States. The signature of relatively arid climates to the west of about 100°W longitude and humid climates east is evident in the RX1day patterns of both observations and models. Terrain organization of RX1day is also strong in the far West, and the key features of maxima in the Cascades, Sierras, and Rockies are fairly well captured at these approximately 50-km resolved model simulations. On larger scales, RX1day magnitudes are greatest in the vicinity of the Gulf Coast and the Southeast. This feature is also well represented in the models, although the magnitude of the RX1day is generally too low along the Gulf Coast.

A key feature of annual RX1day is its distinct seasonality over the contiguous United States. Shown in Fig. 3 (left) is the season during which RX1day events tend to occur based on resolving the annual cycle into six nonoverlapping 2-month periods (January/February, March/April, etc.). The timing of the wettest day tends to conform to the seasonal cycle of climatological mean precipitation itself, notwithstanding that heavy daily rains also occur in warm season convection. Over the far West, the wettest days are observed in late fall and winter, whereas a late spring maximum is found over most of the Great Plains (top). These timings are realistically simulated in each of the three models used herein (lower three panels). Likewise, over much of the Northeast and mid-Atlantic, an early fall (September/October) preference for RX1day occurrence is seen in observations, a feature also evident in most of the models. However, a fall maximum that also occurs over the Southeast is not as well captured in the models, in part owing to contributions from tropical storms whose simulation is deficient in the models used herein. Larger model discrepancies also arise in areas experiencing less distinct wet seasons (e.g., the Ohio Valley). Here, the RX1day occurrences have only a modest preference between adjacent seasons, and thus sampling alone can account for some of the differences between observations and models.

In all three models, summer (July/August) occurrences of RX1day are much less frequent than observed. This is especially noteworthy over Arizona and New Mexico where the heaviest rain days tend to be observed during their summer monsoon season, but are more likely to occur in the cold season associated with wintertime cyclones in the models. This bias arises in part because the models are too wet over the American Southwest during winter, whereas the monsoon rains fail to penetrate as far northward into the American Southwest in summer (not shown). The upper Midwest also tends to experience the wettest rain days in July/August, rather than in late spring as is simulated in the models. This region is prone to heavy rain events from mesoscale convective systems, the occurrences of which are poorly simulated in climate models that rely on convective parameterization (e.g., Prein et al. 2017) as is the case of each of the models used herein.

4. The U.S. pattern of heavy daily precipitation change

a. The signal of historical U.S. RX1day change

The observed change pattern of U.S. heavy daily precipitation is noteworthy for its spatial diversity characterized by large increases over the East and decreases over the West (Fig. 4, top). Results are shown for spatially aggregated changes over 18 USGS water resource regions so as to reduce the noise inherent at the grid point scale, but also to provide a

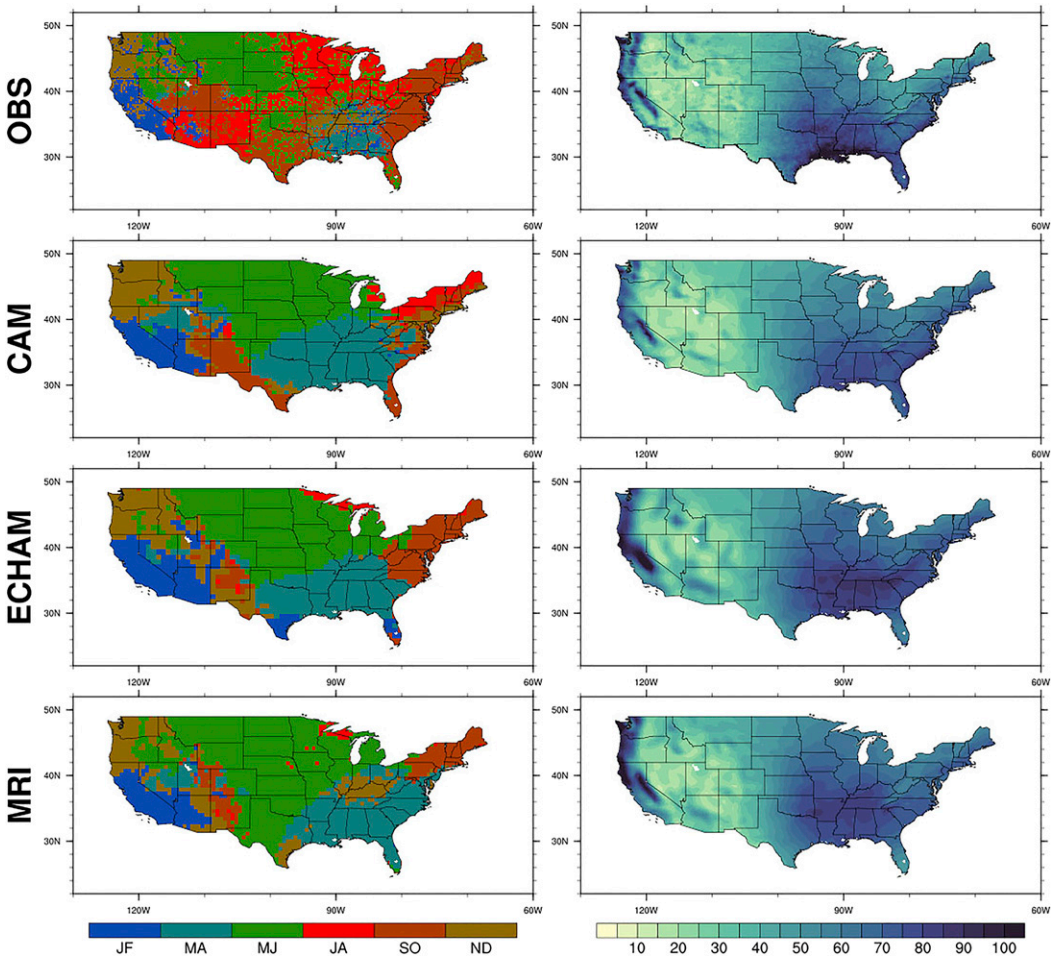

FIG. 3. (right) Magnitude of the climatological wettest day (RX1day; mm) and (left) seasonality for the occurrence for RX1day in (top to bottom) observations, CAM, ECHAM, and MRI simulations. Observations based on 1948–2018 period, and models based on the ensemble average of AMIP simulations for 1979–2018 for CAM and ECHAM, and for 1979–2010 for MRI.

finer granularity than the seven large-scale U.S. regions used to summarize observed heavy precipitation changes in the National Climate Assessment (USGCRP 2018, see their Fig. 2.7). Grid-level magnitude changes in RX1day are averaged for the various regions, and then expressed as a percentage change for the region as a whole. The magnitude of percentage increases for the mid-Atlantic basin is about 25%, while adjacent river basins over New England and the Great Lakes area have observed 15% increases. Broad-scale 10% increases in RX1day have occurred over the Ohio River basin, and the upper and lower Mississippi River catchments. RX1day changes are considerably smaller from the Missouri River basin westward with decreases observed over most of the West including the upper Colorado River, the Pacific Northwest, the Great Basin, and the California basin where a 10% decline is observed. The RX1day change pattern since the mid-twentieth century is similar to that since the beginning of the twentieth century based using a sparser network of historical GHCN daily data beginning in 1901 (see Fig. S1).

This spatial diversity in heavy daily precipitation trends is superposed on an overall nationally averaged intensification. The recent 20-yr period compared to the mid-twentieth century has experienced a 6% increase in RX1day magnitudes, dominated by the much greater rises over the East. The national-scale change compares to a similar 6% increase in annual column precipitable water averaged over the United States (PW; Fig. 4, bottom[1]), close to a Clausius-Clapeyron scaling given the observed ~0.9°C rise in global mean surface temperature since 1950. All regions of the United States have experienced PW increases, implying that the reversal in sign of

[1] The common period for the reanalysis products begins in 1958, and the reference period for PW change is 1958–1977, rather than the 1948–67 period used for RX1day. We note that there is little qualitative difference when the RX1day changes are calculated using a 1958–77 reference. Figure 4 (bottom) uses the average of NCEP–NCAR, JRA-55, and 20thCRv3 products.

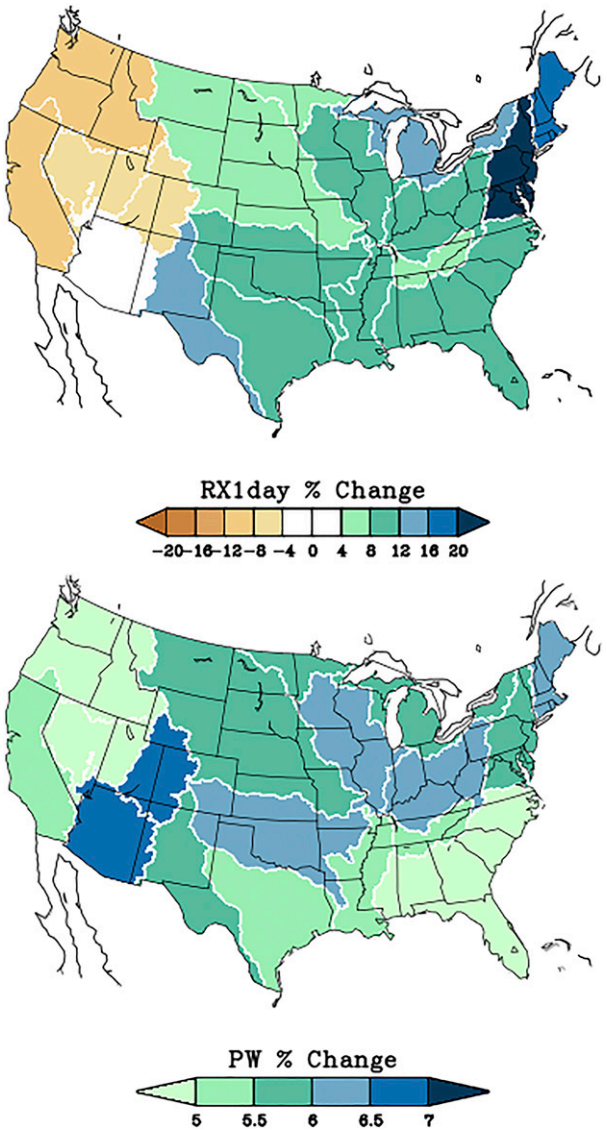

FIG. 4. (top) The observed changes in wettest day of the year (RX1day) and (bottom) column precipitable water (PW). RX1day change calculated as the difference of (1999–2018) minus (1948–67). PW change calculated as the difference of (1999–2018) minus (1958–77). RX1day and PW change are calculated at grid scales, aggregated to the basin scales, and then expressed as the percentage difference relative to the mid-twentieth-century climate. Map outlines are of the 18 USGS major river basins.

RX1day trends when transecting from the eastern to the western United States is broadly inconsistent with notions of thermodynamic control that is implied by the PW change pattern.

We turn to the climate model simulations in order to understand these observed changes and to more rigorously quantify the overall effect of historical climate change forcing on U.S. heavy daily precipitation. Figure 5 shows the ensemble mean differences between factual and counterfactual simulations of annual PW (left) and RX1day (right). All three models exhibit atmospheric moisture increases across the contiguous United States with modestly larger increases over the northern and eastern sections, the patterns and magnitudes of which are in general agreement with the reanalysis estimates of observed change. For national averages, the simulations yield 7%, 6%, and 7% increases in precipitable water for CAM, ECHAM, and MRI models, respectively. Again, these increases in water vapor availability are consistent with expectations of global warming and the rise in global surface temperature of 0.8°–0.9°C occurring in the factual relative to counterfactual simulations.

The wettest day of the year becomes wetter under climate change forcing over most regions of the United States in each of the model ensembles (Fig. 5, right). For averages over the contiguous United States, increases are 2%, 5%, and 3% for CAM, ECHAM, and MRI, respectively. These are smaller than the simulated increases in water vapor availability, consistent with CMIP model results that have also found extreme daily precipitation over the extratropics to increase less rapidly than available atmospheric moisture content (O'Gorman and Schneider 2009). There are several possible physical reasons. One is that air masses in which extreme midlatitude precipitation occurs are often warmer than climatological local conditions due to advection, and these source regions respond to global warming differently (O'Gorman and Schneider 2009). A second factor, quantified in O'Gorman and Schneider (2009), is that the rate of condensation depends on vertical gradients of saturation specific humidity which can increase by as little as half the rate of saturation specific humidity itself. Another is a decline in near-surface relative humidity over the continental United States occurring in our model experiments (not shown), a feature also noted in observations (e.g., Willett et al. 2014) and other global model simulations (Byrne and O'Gorman 2016). A reduction in lower tropospheric relative humidity has been argued to reduce precipitation efficiency (e.g., Ye et al. 2014; Cheng et al. 2018) in that greater airmass ascent is required to achieve condensation, which would thereby occur at cooler temperatures thus offsetting some of the effects of increased column precipitable water.

The model signals of heavy daily precipitation change reveal considerable spatial heterogeneity, especially for ECHAM and MRI. The largest increases occur east of the Missouri River basin ranging from 5% to 10%. (Fig. 5, right). Smaller increases are simulated across the West, with a signal of decreased intensity over the Southwest. ECHAM and MRI exhibit similar RX1day sensitivities across the United States as a whole, and their ensemble mean signals better agree with the pattern of strong west–east contrast evident in the observations. It is worth noting that simulated declines in each model occur over the Southwest, whereas the largest observed decline (since 1948) occurs over the Pacific Northwest. While biases in the models' RX1day regional sensitivities may exist, sampling uncertainty of the regional pattern is also to be noted, for instance as is evident by a more pronounced Southwest decline in observed trends calculated from 1901 (see Fig. S1) and by a strong sampling uncertainty in centennial-scale changes among individual model realizations that are discussed further below. The CAM RX1day sensitivity is by

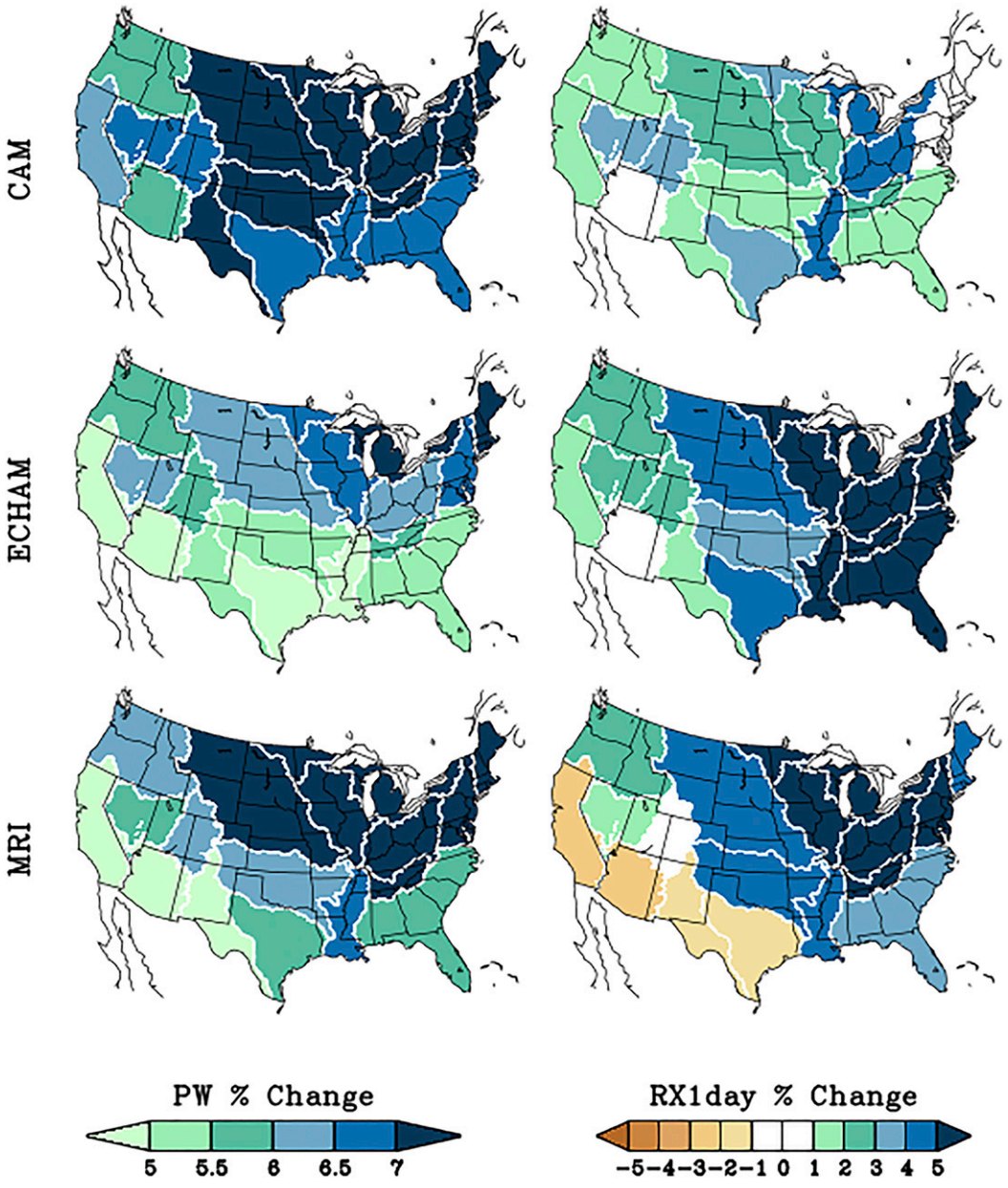

FIG. 5. (left) The simulated changes in column precipitable water (PW) and (right) wettest day of the year (RX1day). Shown are the ensemble mean changes of the factual minus counterfactual simulations of 1999–2018 for the (top) CAM, (middle) ECHAM, and (bottom) MRI models. RX1day and PW change calculated are calculated at model grid scales, aggregated to the basin scales, and then expressed as the percentage difference relative to the models' counterfactual climate. Maps and contouring are as for observations except that the RX1day scale is reduced compared to that in Fig. 4.

contrast generally weaker and more spatially homogeneous, and its virtual absence of change over the mid-Atlantic basin contrasts strikingly with observations. These model structural differences and their origins are diagnosed and discussed further in sections 4b and 4c. Here it is sufficient to note that none of the models generate a forced signal of intensification as large as the 25% increase observed in the mid-Atlantic basin, either over that basin or over any other U.S. river basin (note that the contour range of simulated RX1day change in Fig. 5 has been reduced to facilitate comparison with observations). Nor do they generate a forced signal of decline as large as the 10% decrease over the far West. Underestimates of observed amplification of daily rainfall extremes have been previously noted in CMIP models and are typically attributed to coarseness of spatial resolution (e.g., Allan and Soden 2008). Yet, results of section 3 suggest the models used herein credibly

produce the climatological intensity of extreme precipitation over many U.S. regions, although biases were also identified especially where convection is an important contributor. The role of sampling variability, to be assessed in section 4b, has been recognized as important which can also account for differences between regional intensification in historical trends compared to forced responses in ensemble simulations—even for centennial scales (Fischer et al. 2014).

To summarize the key finding regarding the forced responses, potential model biases notwithstanding, the sensitivity of U.S. RX1day to climate change forcing over the last century is spatially diverse, being characterized by larger increases in the East compared to the West. Such a pattern is analogous to observed trends for data beginning in 1901, when station coverage was sparser and less abundant, and since 1948 when more complete observations became available. Using the observed trend pattern of RX1day since 1948, we find positive spatial congruences (correlations) of the modeled U.S. signals of 0.5 (0.2), 0.7 (0.6), and 0.5 (0.3) for CAM, ECHAM, and MRI, respectively. The congruences, which measure the full field similarity, are higher because the models and observations each produce a nationally averaged increase in RX1day intensity. Importantly, upon removing this overall increase, there continues to be considerable spatial agreement indicating that the regional contrasts in observed trends may be interpretable as an articulation of climate change. A strong west–east contrast is particularly evident in simulated change signals of ECHAM5 and MRI after removing their contiguous U.S. increases (see Fig. S3). Structural uncertainty in the forced signals is however also noteworthy, with one of the models (CAM) exhibiting weaker RX1day responses to climate change and less spatial diversity in its U.S. signal.

b. *Robustness of U.S. RX1day change pattern to natural variability*

The spatial agreement between the historical RX1day trend pattern and our simulated ensemble mean response patterns may be an artifact of noise in the single observed record rather than strong evidence for nature's climate change sensitivity. To address this sampling issue, the parallel-pair constructs of our model simulations are leveraged to calculate spatial agreements between each factual versus counterfactual difference map and the observed trend, the results of which are summarized by histograms in Fig. 6 comprised of 364 CAM, 2500 ECHAM, and 625 MRI change map comparisons. The vast majority of the simulated change maps are congruent with the observed pattern (top curves). Upon removing the area-averaged values, the histograms of the resulting correlations for ECHAM and MRI affirm that the majority of simulated model changes continue to agree in pattern with the observed change (lower curves). The population samples of CAM correlations show little systematic preference for a spatial pattern agreeing with observations, and consistent with the results of Fig. 5 its histogram departs significantly from those of the other two models. We interpret these results, in aggregate across the three models, to indicate that the positive congruence and correlation of the historical RX1day trend pattern with the simulated ensemble mean responses (most evident in the ECHAM and MRI simulations) is not an artifact of sampling noise, but expresses the presence of a climate change signal.

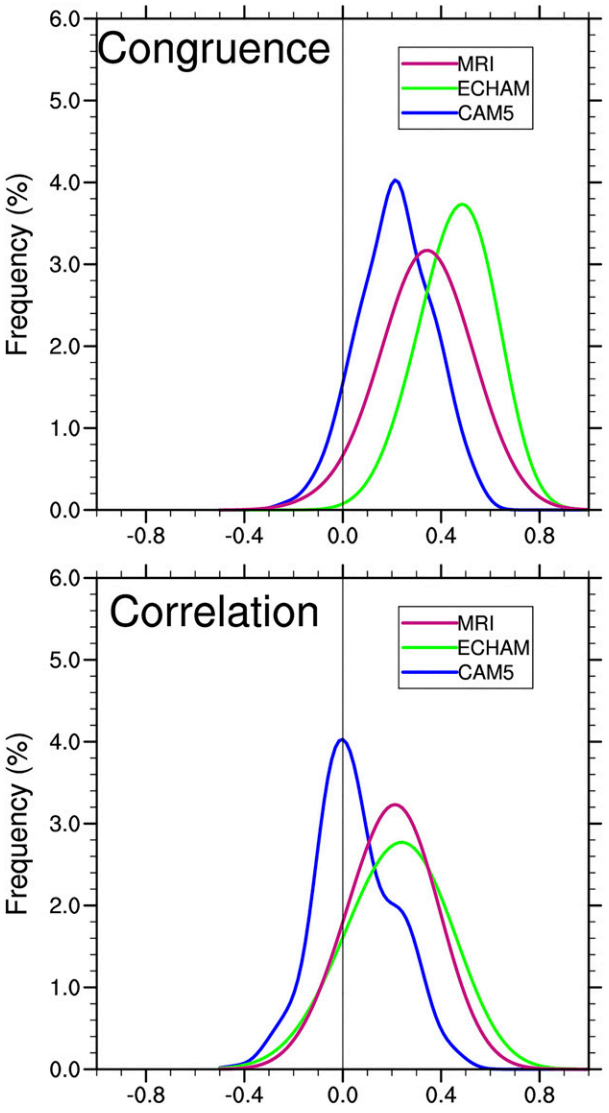

FIG. 6. Histograms of the spatial pattern agreement between observed and model-simulated RX1day changes for the contiguous U.S. region based on (top) congruence and (bottom) correlation. Data are compared on a 5° latitude × 5° longitude grid. Histograms are derived from 324 CAM (blue), 2500 ECHAM5 (green), and 625 MRI (purple) map comparisons with the observed change map. The probability distribution functions are nonparametric curves constructed using the R software program, which utilizes a kernel density estimation and a Gaussian smoother.

We next inquire into the magnitudes of RX1day changes at regional scales and how strongly those are determined by historical climate change forcing since the early twentieth century. Figure 7 examines the statistics of changes for each of the models averaged over the mid-Atlantic basin of dramatic observed increases and over the California basin of observed declines. The changes in these two regions anchor the west–east

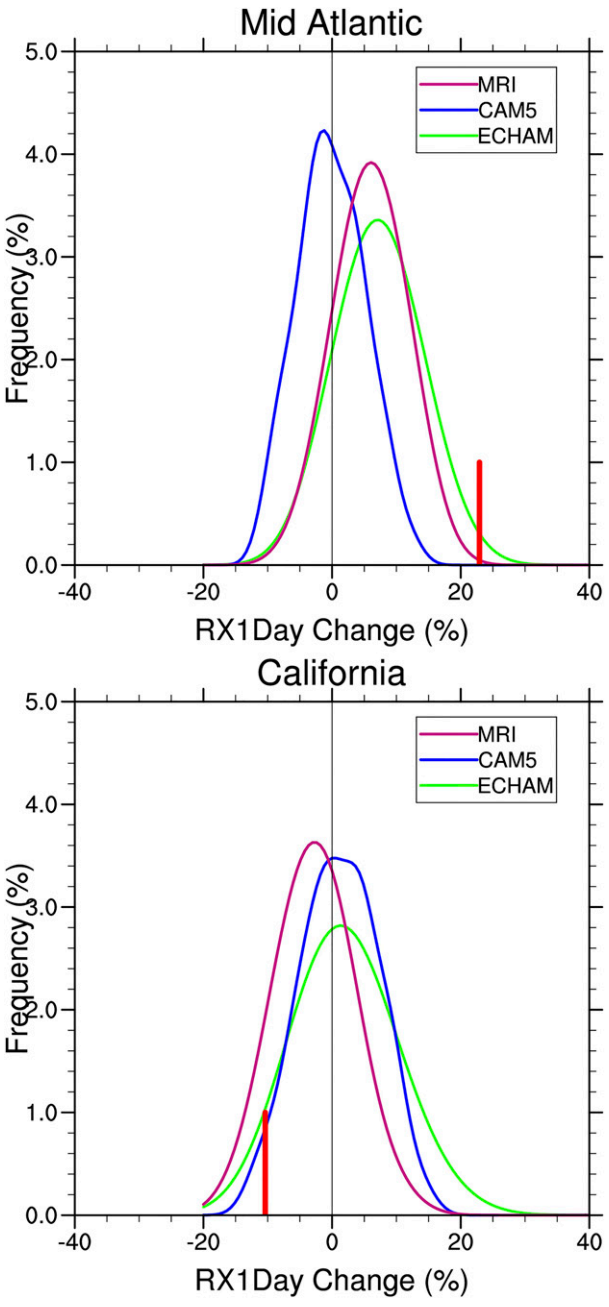

FIG. 7. Histograms of simulated RX1day change (%) for drainage basins of the (top) mid-Atlantic and (bottom) California. Histograms are derived from 324 CAM (blue), 2500 ECHAM5 (green), and 625 MRI (purple) paired differences of factual vs counterfactual experiments. Bold red tic marks denote the observed RX1day changes. The probability distribution functions are nonparametric curves constructed using the R software program, which utilizes a kernel density estimation and a Gaussian smoother.

gradient of observed RX1day trends of Fig. 4. The probability distributions exhibit considerable spread for both basins in each of the three models. The effect of internal noise could thus alone yield appreciable change in RX1day magnitudes even on the centennial time scale.

TABLE 3. Standardized RX1day mean differences for factual vs counterfactual experiments. Standardized values significant at the 5% level are boldface and italic.

River basin	CAM	ECHAM	MRI
New England	−0.1	***1.0***	***1.0***
Mid-Atlantic	0.	***1.3***	***1.2***
South Atlantic Coast	0.3	***1.6***	***0.6***
Great Lakes	***1.0***	***2.3***	***2.5***
Ohio	***1.3***	***1.1***	***2.0***
Tennessee	***0.5***	***1.1***	***1.1***
Upper Mississippi	***0.7***	***1.5***	***2.6***
Lower Mississippi	***0.5***	***1.1***	***0.9***
Souris–Red–Rainy	***0.5***	***1.1***	***1.5***
Missouri	***0.7***	***1.2***	***1.5***
Arkansas–Red–White	***0.5***	***0.8***	***1.2***
Texas Gulf Coast	***0.5***	***0.7***	−0.2
Rio Grande	0.2	0.3	−0.3
Upper Colorado	***0.6***	***0.7***	0.2
Lower Colorado	0.	−0.1	***-0.4***
Great Basin	***0.7***	***0.5***	***0.4***
Pacific Northwest	***0.4***	***0.6***	***0.8***
California	0.2	***0.3***	***-0.5***

For the mid-Atlantic (Fig. 7, top), the majority of ECHAM and MRI simulations yield increases in RX1day values, indicating a constraining effect of climate change on the directionality of heavy rainfall responses. The histograms of ECHAM and MRI both indicate that the most likely magnitude increase in recent decades compared to the early twentieth century is about 8%. These signals correspond to about 1.2 standardized departures (see Table 3), which are statistically significant at the 5% level. In contrast, the CAM histogram is again significantly different from the other models, indicating no preference for either increased or decreased RX1day magnitudes in the mid-Atlantic. The spread among the samples of centennial change in RX1day is very similar among the three models (standard deviation of RX1day percentage change is 5%–6%). Thus, an increase as great as the 25% observed intensification, while clearly far in excess of the climate change signal as per each of our models, can best be reconciled with an interpretation of strong internal variability superposed on a moderate forced change. To be sure, relatively few simulated samples achieve change magnitudes as large as observed (red tic mark), and then only in the two models having larger signals—the CAM statistics indicate that a 25% intensification could not have occurred over the last century. The model results, taken collectively, imply that a particularly large articulation of internal variability most likely operated in the mid-Atlantic basin in order to account for its outsized RX1day change relative to other river basins in the United States. We cannot rule out the possibility that a dimension of forcing that we did not investigate, such as the change pattern in SSTs, or that model biases in sensitivities to forcing have adversely affected responses, especially at regional scales. We should note, however, that the outlier behavior of RX1day changes vis-à-vis the model statistics over this mid-Atlantic basin is not obviously symptomatic of a bias in either model sensitivity to

forcing or intensities of simulated internal variability. This is suggested by the fact that observed change magnitudes over all individual 18 U.S. major river basins reside consistently within the combined model ranges in a manner expected from sampling (see Fig. S2).

For the California basin, the three models are in somewhat closer agreement with each other and reveal no appreciable signal of RX1day change. The most likely value of the sampling distribution, as indicated by the similar statistical modes of the CAM and ECHAM PDFs, is effectively no difference in heavy daily precipitation under climate forcing of the early twenty-first century compared to the early twentieth century, whereas the MRI model indicates a mean decline of 0.5 standardized departures which is significant at the 5% level. The observed trend toward moderate declining RX1day magnitudes is therefore quite consistent with these model indications. The internal variability in RX1day trends over the California basin (~6%) is comparable to that over the mid-Atlantic basin (~5%), and thus the small model signals in the former region are mostly overwhelmed by the magnitude of noise.

c. *Climate change effects on atmospheric dynamics and the western U.S. RX1day decline*

Given the prevailing drought conditions post-2000, it might not be surprising that western U.S. extreme daily precipitation has become less intense in recent years. Sometimes referred to as the Millennium Drought, its intensity is believed to have rivaled multidecadal western U.S. dry spells in the paleoclimatic record (e.g., Williams et al. 2020). Nonetheless, the observed decline in heavy daily precipitation intensities over large portions of the West, despite increasing PW, is remarkable for its striking contrast to the large increases over the eastern United States and most midlatitude locations (e.g., Dittus et al. 2016). The physical basis for this weak signal of the West is a dynamical effect, which acts in opposition to the increase that would have been expected from thermodynamics of global warming alone. The new experimental results presented herein make a strong case that the absence of an observed change in RX1day over the West is likely a dynamical signal of climate change at least for the global SST warming patterns used here, and has not been merely a sampling artifact of internal dynamical variability.

To illustrate, we focus on the winter season (January–February) when the wettest day of the year occurs over much of the West (see Fig. 3), and thus is most relevant for understanding the cause for the weak western U.S. RX1day change signal in the models. The 1999–2018 period that captures the Millennium Drought has witnessed sustained below normal precipitation over much of the West (Diaz and Wahl 2015; Williams et al. 2020), and as shown in Fig. 4 has experienced reduced RX1day intensities. Both mean and extreme precipitation has responded to a tropospheric circulation pattern consisting of 700 hPa anomalous high pressure over the Pacific Northwest (Fig. 8, top). Reanalysis data show that this circulation pattern has induced anomalous downward vertical motion in the West (not shown), which has likely inhibited both the mean precipitation and also the intensity of wintertime daily extremes (see e.g., O'Gorman and Schneider 2009).

The ensemble CAM and ECHAM responses[2] to climate change are each characterized by a similar atmospheric circulation pattern over the Pacific Northwest that each resemble the observed change (Fig. 8, bottom), with anomalous high pressure over that region which appears to be part of a wave train resembling elements of the classic Pacific–North American circulation pattern (Barnston and Livezey 1987). Analysis of the simulated midtropospheric mean vertical motion changes in winter reveals a trend toward greater sinking motion (not shown), which would inhibit the occurrence of extreme precipitation.

Our interpretation is that the weak signal of RX1day change in the West is not due to the absence of sensitivity to climate change per se. Rather, the model experiments indicate it is due to the tendency for climate change's thermodynamic driving toward increased heavy precipitation to be compensated by climate change's regional dynamical driving toward decreased heavy precipitation. Analogous compensating effects have been noted in future projections of midlatitude regional extreme precipitation change, in particular over the Mediterranean region (Pfahl et al. 2017). However, the Pfahl et al. study that decomposed projected future changes in heavy daily precipitation into thermodynamic and dynamic contributions does not show a dynamical suppression over the West. Whether the suppression identified herein during the historical period is particular to a sensitivity to observed changes in SSTs that drive our atmospheric models that is distinct from SST effects in coupled model projections is unclear. However, it is evident that such an effect has been an important factor leading to the strong spatial heterogeneity in U.S. heavy precipitation trends since the early twentieth century.

A further comparison of the model circulation responses reveals downstream differences, in particular a high pressure in CAM's response that extends over the eastern United States, while such a feature is absent in the ECHAM response and absent also in the observed change pattern. This high pressure in CAM would be expected to also inhibit heavy precipitation in the eastern United States. These model structural differences in wavy circulation responses to climate change thus appear to be physically consistent with differences in the spatial diversity of U.S. RX1day responses among the models studied herein. It is important to note, however, that the wettest day of the year in the mid-Atlantic occurs in late summer not late winter, and these winter circulation response discrepancies may be immaterial to determining the U.S. RX1day change map overall. Since the mid-Atlantic experiences its RX1day occurrences in September/October (see Fig. 4), we therefore also examined that season's 700-hPa height responses. The ensemble averaged CAM simulations yield a regionally distinct and strong anticyclonic circulation over the

[2] Results for the MRI model circulation responses at 700 hPa are not presented because the geopotential height data were unavailable to this project. However, sea level pressure data were available for all three models, and their factual versus counterfactual SLP responses were similar to each other, consisting of anomalously high surface pressure across the Gulf of Alaska and western Canada analogous to the tropospheric circulation pattern of Fig. 8.

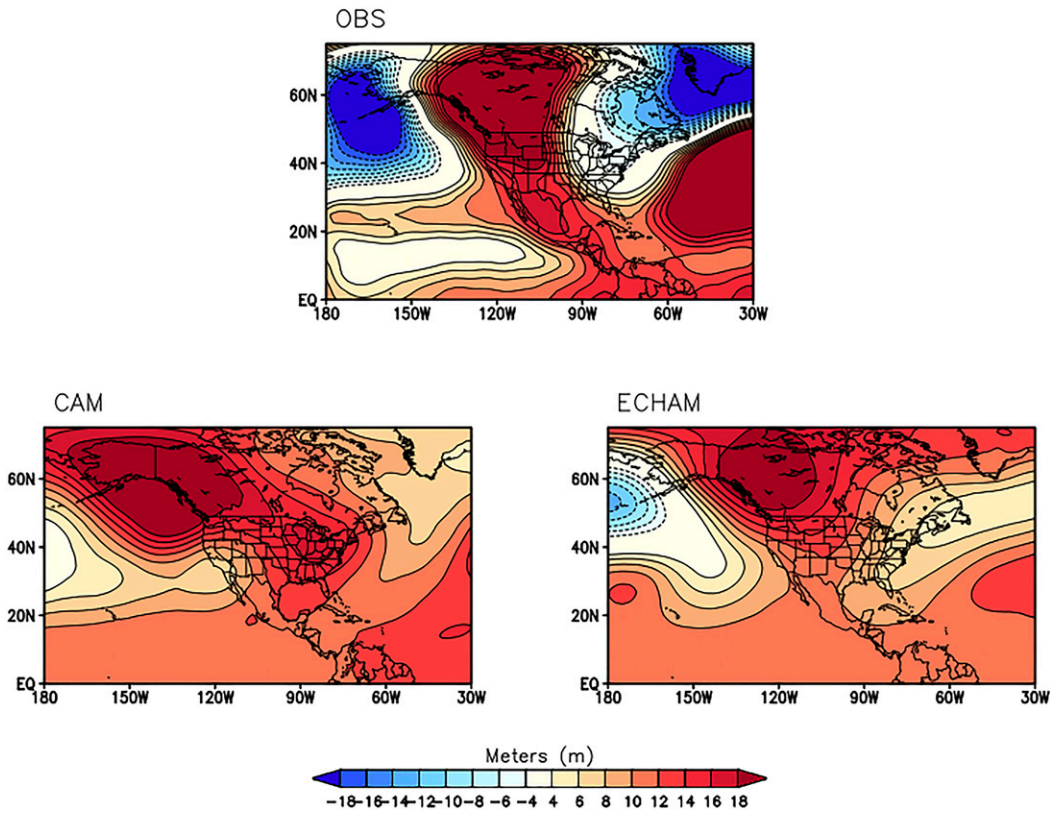

FIG. 8. (top) Observed January/February 700-hPa height change, and the ensemble mean simulated January/February 700-hPa height change for (bottom left) CAM and (bottom right) ECHAM. Contour interval is 2 m. The observed height change is calculated as the difference of (1999–2018) minus (1948–67) based on NCEP–NCAR reanalysis. The simulated changes are the difference of the factual minus counterfactual ensemble means.

U.S. Northeast, for which no counterpart is found in our other models or in observations (see Fig. S4). The weak RX1day ensemble mean response over the Northeast in CAM is thus likely due to dynamical suppression compensating an otherwise thermodynamic increase. This signal of an anticyclonic circulation and its related subsidence appears not to be consistent with observations (which could stem merely from sampling), but it is also inconsistent with CMIP5 model projections for 1950–2100 that reveal a dynamical enhancement of extreme precipitation over the East (Pfahl et al. 2017).

5. Summary and concluding remarks

Annual maximum one-day precipitation (RX1day) has increased 15%–25% in magnitude over parts of the eastern United States since the early and mid-twentieth century, while a 10% intensity decline has occurred over the far western United States Yet all regions of the United States have experienced column precipitable water (PW) increases, implying that the observed reversal in sign of RX1day trends when transecting from east to west is inconsistent with notions of thermodynamic control tied to water vapor availability.

Using atmospheric model simulations, we find that U.S. RX1day events respond to climate change forcing differently over the eastern compared to the western United States. Experiments using three different models indicate an aggregate sensitivity to forcing changes spanning the last century that consists of 5%–10% increases in RX1day intensity over the East and little or no change over the West. The resulting spatially diverse pattern of climate change impacts was found to be particularly prominent in two of the three models used herein, and each model's signal was positively correlated with the observed trend pattern.

Two factors are argued to be mainly responsible for the remarkable spatial diversity of observed RX1day changes. First, the absence of appreciable RX1day increases over the West is attributed to a dynamical effect of the observed centennial-scale trends in SST, sea ice, and atmospheric composition. This consists of a forced circulation pattern during winter—the season of RX1day occurrences in the West—anchored by anomalous high pressure over the Gulf of Alaska and the Pacific Northwest. The model signal generally resembles the observed western North American circulation anomaly pattern that has prevailed in recent decades. Through its driving of large-scale sinking motion over the West, extreme precipitation has been dynamically suppressed, an effect largely compensating increases anticipated from thermodynamic effects of global warming to date.

A second factor is sampling variability. Our model results indicate the large observed RX1day increases over the mid-Atlantic that anchor the U.S. pattern of zonal contrast can be attributed to strong internal atmospheric variability rather than being due to a particular heightened regional climate change sensitivity. The basis for this interpretation is rooted in our model results showing large amplitude RX1day changes due to internal atmospheric variability on centennial time scales. The magnitude of this internally generated variability was comparable to the forced signal of increased RX1day in the East, and far exceeded the much weaker forced signals in the West. These experimental results—common among all three models studied herein—thus support an explanation that the striking 25% increase of RX1day intensity in the mid-Atlantic basin has most likely been due to a combination of moderate forced increases comingled with a strong articulation of internal atmospheric variability.

An overarching purpose for explaining the historical changes in extreme daily precipitation is to apply that knowledge to expectations for coming decades. Having found evidence that historical changes in boundary forcings favored larger RX1day increases in the eastern than in the western United States, a reasonable question is whether our results support a projection that such regional differences will continue to prevail, or perhaps intensify as global warming increases. Our view is that such an outcome constitutes a plausible scenario for near-term (decadal) conditions based simply on the continuation of the long-term trend patterns. Because our model sensitivities are robust to using the zonal mean trend or the spatial pattern (MRI) of SST trend, we put more credence in an anthropogenic origin of these trends and thus anticipate some degree of at least near-term persistence. But confidence must be tempered by the reality of internal variability, and also by structural uncertainty in simulated regional details of the forced signal of RX1day change.

In that regard, it is important to recognize some of the limitations of the modeling results presented. It was noted, for instance, that one of the models used herein was unable to simulate RX1day increases as large as observed in the mid-Atlantic region within its population sample, while the other two models required invoking a very large-amplitude occurrence of natural variability. One aspect concerns model differences in dynamical sensitivities to climate change forcings. Another concerns the character of internal atmospheric variability itself. Empirical analysis has shown that an important contributor to the observed mid-Atlantic RX1day increases has been tropical cyclones occurring more frequently over the Northeast during recent decades (Kunkel et al. 2012). Kunkel et al. (2010) also suggest that the increase in U.S. heavy rainfall amounts due to tropical cyclones is not due to frequency increases alone but also because such storms are producing heavier rainfall. There is growing evidence that anthropogenic climate change is contributing to heavier rainfall in tropical cyclones (e.g., Risser and Wehner 2017; van Oldenborgh et al. 2017), even while attribution of changes in the frequency or tracks of Atlantic tropical storms is challenged by their large intrinsic decadal variability and the smallness of the human-induced climate change impact to date (Knutson et al. 2019). Insofar as all the models used herein have inadequate resolution to generate realistic tropical cyclone statistics, they underestimate the internal variability of RX1day events in the mid-Atlantic and other U.S. regions prone to tropical cyclone–related rains. The models are thus likely missing a contribution to variability of extreme rainfall in the Northeast that has been known to be a factor in recent decades. Recognizing the potency of unforced atmospheric dynamics, a scenario in which internal variability could mute if not reverse the observed upward trend in eastern U.S. RX1day magnitudes cannot be discounted.

A question also turns to the RX1day climate change signal itself. The spatial diversity of the U.S. signal estimated in our experiments was based on a particular treatment of boundary forcings, and the issue is whether our results are especially dependent on the manner in which those were constructed for the historical record, and also whether that historical sensitivity will be robust to future forcing changes. Concerning the first issue, the simulated sensitivity of U.S. RX1day to climate change depends to a large degree on the so-called global warming pattern, which we removed from the actual ocean surface boundary states in order to estimate climate forcing absent human influence (in addition to adjustments made to atmospheric chemical composition and aerosols). Some measure of robustness was provided by employing two observational estimates of the global SST warming, each derived from historical observations: one based on the zonally averaged trends and the other based on a two-dimensional field of the trend. There is also uncertainty in the pattern of long-term trends among different gridded SST datasets, due largely to differences in reconstruction and interpolation methodology. This uncertainty can be reduced by applying an ENSO filter to the data. When this is done, the residual SST trend for 1900–2010 is quite similar among four datasets used in Solomon and Newman (2012) consisting of a strengthening of the SST gradient across the Indo-Pacific, similar to the unfiltered COBE trend used in the MRI experiments.

Alternatively, CMIP climate models can be used to estimate the SST change patterns, an approach used in other event attribution studies (e.g., Pall et al. 2011; Christidis et al. 2013; Ciavarella et al. 2018). This approach has the benefit of more directly employing a change in lower boundary conditions that can be directly attributed (in the model) to human-induced climate change, whereas the observed change pattern will contain elements of historical internal coupled variability. A weakness of that approach is that CMIP models have considerable biases in their simulations of the tropical Pacific SST climatology and variability. Rescaling of simulated trends can be applied using optimal fingerprinting detection methods (Kay et al. 2011), yet the underlying coupled model biases that determine the fingerprints themselves remain problematic.

Regardless of method, it is important to recognize the limited detectability of a human-induced SST trend over the tropical central and eastern Pacific during the instrumental period (Knutson et al. 2013). Temperature change in this region of the World Ocean is critical for determining the character of regional U.S. climate changes, especially for precipitation patterns (e.g., Shin and Sardeshmukh 2010;

Hoerling et al. 2010, 2016). To be sure, models used herein yielded similar climate signals for U.S. RX1day changes (especially ECHAM and MRI), even though the MRI experiments were subjected to the two-dimensional observed SST change pattern while CAM and ECHAM employed its zonally averaged component only. It is indeed noteworthy that even in experiments that included only a zonally symmetric representation of long-term SST change, a zonally asymmetric wavy response of the atmosphere occurred. Further experimentation is required to untangle the effects of pure, human-induced climate change from effects of internal multidecadal- and centennial-scale SST variability.

Concerning the second issue, projections of twenty-first-century climate change indicate an El Niño–like tropical SST warming pattern in which Indo-Pacific SST gradients weaken, apparently reversing the strengthening that occurred in the instrumental period (e.g., Collins et al. 2010). The effect of this, if such projections verify, is to generate a midlatitude dynamical atmospheric response itself resembling the El Niño teleconnection. This includes increased winter precipitation in California (Allen and Luptowitz 2017) and an associated increase in extreme daily precipitation events (see, e.g., Sillmann et al. 2013). Thus, our result showing a forced signal of no change in RX1day intensity over the West during the instrumental record may be viewed as a transient signal, one that could reverse as dynamical driving together with the overall thermodynamic increases expected from water vapor availability makes extreme rainfall events more intense. Yet, models with particularly poor ENSO variability have tended to exhibit the largest El Niño–like SST expressions of climate change (e.g., Collins et al. 2005), muting confidence in the emergence of such a pattern and its regional impacts.

These matters are ripe for analysis using the new suites of CMIP6 models. Particularly intriguing are experiments of both atmospheric and coupled ocean–atmospheric models that employ appreciably higher spatial resolution in both the atmosphere and ocean than has previously been available for climate studies (Haarsma et al. 2016). The experiments are expected to provide more realistic simulations of variability and may thereby offer more reliable indications of regional climate impacts, especially for extreme events.

Acknowledgments. We acknowledge Dr. Yukiko Imada for providing the data from the MRI3.2 climate simulations that were produced at the Japanese Meteorological Research Institute. We also acknowledge David Allured for generating the ECHAM5 climate simulations in the Physical Sciences Laboratory. The authors thank Dr. Aaron Wang and three anonymous reviewers for their helpful comments on an earlier draft of the paper. The study has also benefited from conversations on this topic with Dr. Randall Dole.

REFERENCES

Allan, R., and B. Soden, 2008: Atmospheric warming and the amplification of precipitation extremes. *Science*, **321**, 1481–1484, https://doi.org/10.1126/science.1160787.

Allen, M., and W. Ingram, 2002: Constraints on future changes in climate and the hydrologic cycle. *Nature*, **419**, 228–232, https://doi.org/10.1038/nature01092.

Allen, R., and R. Luptowitz, 2017: El Niño–like teleconnection increases California precipitation in response to warming. *Nat. Commun.*, **8**, 16055, https://doi.org/10.1038/ncomms16055.

Barlow, M., 2011: Influence of hurricane-related activity on North American extreme precipitation. *Geophys. Res. Lett.*, **38**, L04705, https://doi.org/10.1029/2010GL046258.

Barnston, A. G., and R. E. Livezey, 1987: Classification, seasonality, and persistence of low-frequency atmospheric circulation patterns. *Mon. Wea. Rev.*, **115**, 1083–1126, https://doi.org/10.1175/1520-0493(1987)115<1083:CSAPOL>2.0.CO;2.

Byrne, M. P., and P. A. O'Gorman, 2016: Understanding decreases in land relative humidity with global warming: Conceptual model and GCM simulations. *J. Climate*, **29**, 9045–9061, https://doi.org/10.1175/JCLI-D-16-0351.1.

Chen, M., W. Shi, P. Xie, V. Silva, V. Kousky, R. W. Higgins, and J. E. Janowiak, 2008: Assessing objective techniques for gauge-based analyses of global daily precipitation. *J. Geophys. Res.*, **113**, D04110, https://doi.org/10.1029/2007JD009132.

Cheng, L., M. Hoerling, L. Smith, and J. Eischeid, 2018: Diagnosing human-induced dynamic and thermodynamic drivers of extreme rainfall. *J. Climate*, **31**, 1029–1051, https://doi.org/10.1175/JCLI-D-16-0919.1.

Christidis, N., and Coauthors, 2013: A new HadGEM3-A-based system for attribution of weather- and climate-related extreme events. *J. Climate*, **26**, 2756–2783, https://doi.org/10.1175/JCLI-D-12-00169.1.

——, A. Ciavarella, and P. A. Stott, 2018: Different ways of framing event attribution questions: The example of warm and wet winters in the United Kingdom similar to 2015/16. *J. Climate*, **31**, 4827–4845, https://doi.org/10.1175/JCLI-D-17-0464.1.

Ciavarella, A., and Coauthors, 2018: Upgrade of the HadGEM3-A based attribution system to high resolution and a new validation framework for probabilistic event attribution. *Wea. Climate Extremes*, **20**, 9–32, https://doi.org/10.1016/j.wace.2018.03.003.

Cionni, I., and Coauthors, 2011: Ozone database in support of CMIP5 simulations: Results and corresponding radiative forcing. *Atmos. Chem. Phys.*, **11**, 11 267–11 292, https://doi.org/10.5194/acp-11-11267-2011.

Collins, M., and Coauthors, 2005: El Niño– or La Niña–like climate change? *Climate Dyn.*, **24**, 89–104, https://doi.org/10.1007/s00382-004-0478-x.

——, and Coauthors, 2010: The impact of global warming on the tropical Pacific Ocean and El Niño. *Nat. Geosci.*, **3**, 391–397, https://doi.org/10.1038/ngeo868.

Compo, G. P., and Coauthors, 2011: The Twentieth Century Reanalysis Project. *Quart. J. Roy. Meteor. Soc.*, **137**, (654), 1–28, https://doi.org/10.1002/qj.776.

Deser, C., A. S. Phillips, M. A. Alexander, and B. V. Smoliak, 2014: Projecting North American climate over the next 50 years: Uncertainty due to internal variability. *J. Climate*, **27**, 2271–2296, https://doi.org/10.1175/JCLI-D-13-00451.1.

Diaz, H. F., and E. R. Wahl, 2015: Recent California water year precipitation deficits: A 440-year perspective. *J. Climate*, **28**, 4637–4652, https://doi.org/10.1175/jcli-d-14-00774.1.

Dittus, A. J., D. J. Karoly, S. C. Lewis, and L. V. Alexander, 2015: A multiregion assessment of observed changes in the areal extent of temperature and precipitation extremes. *J. Climate*, **28**, 9206–9220, https://doi.org/10.1175/jcli-d-14-00753.1.

——, ——, ——, ——, and M. G. Donat, 2016: A multiregion model evaluation and attribution study of historical changes in the area affected by temperature and precipitation extremes.

J. Climate, **29**, 8285–8299, https://doi.org/10.1175/JCLI-D-16-0164.1.

Easterling, D. R., and Coauthors, 2017: Precipitation change in the United States. *Climate Science Special Report: Fourth National Climate Assessment*, D. J. Wuebbles et al., Eds., Vol. I, U.S. Global Change Research Program, 207–230, https://doi.org/10.7930/J0H993CC.

Emori, S., and S. J. Brown, 2005: Dynamic and thermodynamic changes in mean and extreme precipitation under changed climate. *Geophys. Res. Lett.*, **32**, L17706, https://doi.org/10.1029/2005GL023272.

Fischer, E. M., and R. Knutti, 2014: Detection of spatially aggregated changes in temperature and precipitation extremes. *Geophys. Res. Lett.*, **41**, 547–554, https://doi.org/10.1002/2013GL058499.

——, and ——, 2016: Observed heavy precipitation increase confirms theory and early models. *Nat. Climate Change*, **6**, 986–991, https://doi.org/10.1038/nclimate3110.

——, J. Sedlacek, E. Hawkins, and R. Knutti, 2014: Models agree on forced response pattern of precipitation and temperature extremes. *Geophys. Res. Lett.*, **41**, 8554–8562, https://doi.org/10.1002/2014GL062018.

Haarsma, R. J., and Coauthors, 2016: High Resolution Model Intercomparison Project (HighResMIP v1.0) for CMIP6. *Geosci. Model Dev.*, **9**, 4185–4208, https://doi.org/10.5194/gmd-9-4185-2016.

Hirahara, S., M. Ishii, and Y. Fukuda, 2014: Centennial-scale sea surface temperature analysis and its uncertainty. *J. Climate*, **27**, 57–75, https://doi.org/10.1175/JCLI-D-12-00837.1.

Hoerling, M., J. Eischeid, and J. Perlwitz, 2010: Regional precipitation trends: Distinguishing natural variability from anthropogenic forcing. *J. Climate*, **23**, 2131–2145, https://doi.org/10.1175/2009JCLI3420.1.

——, ——, ——, X. Quan, K. Wolter, and L. Cheng, 2016: Characterizing recent trends in U.S. heavy precipitation. *J. Climate*, **29**, 2313–2332, https://doi.org/10.1175/JCLI-D-15-0441.1.

——, J. Barsugli, B. Livneh, J. Eischeid, X. Quan, and A. Badger, 2019: Causes for the century-long decline in Colorado River flow. *J. Climate*, **32**, 8181–8203, https://doi.org/10.1175/JCLI-D-19-0207.1.

Hurrell, J., J. Hack, D. Shea, J. Caron, and J. Rosinski, 2008: A new sea surface temperature and sea ice boundary dataset for the Community Atmosphere Model. *J. Climate*, **21**, 5145–5153, https://doi.org/10.1175/2008JCLI2292.1.

Kalnay, E., and Coauthors, 1996: The NCEP/NCAR 40-Year Reanalysis Project. *Bull. Amer. Meteor. Soc.*, **77**, 437–471, https://doi.org/10.1175/1520-0477(1996)077<0437:TNYRP>2.0.CO;2.

Karl, T. R., and R. W. Knight, 1998: Secular trends of precipitation amount, frequency, and intensity in the United States. *Bull. Amer. Meteor. Soc.*, **79**, 231–241, https://doi.org/10.1175/1520-0477(1998)079<0231:STOPAF>2.0.CO;2.

Kay, A., S. Crooks, P. Pall, and D. Stone, 2011: Attribution of autumn/winter 2000 flood risk in England to anthropogenic climate change: A catchment-based study. *J. Hydrol.*, **406**, 97–112, https://doi.org/10.1016/j.jhydrol.2011.06.006.

Kirchmeier-Young, M., and X. Zhang, 2020: Human influence has intensified extreme precipitation in North America. *Proc. Natl. Acad. Sci. USA*, **117**, 13 308–13 313, https://doi.org/10.1073/pnas.1921628117.

Knutson, T., F. Zeng, and A. Wittenberg, 2013: Multimodel assessment of regional surface temperature trends: CMIP3 and CMIP5 twentieth-century simulations. *J. Climate*, **26**, 8709–8743, https://doi.org/10.1175/JCLI-D-12-00567.1.

——, and Coauthors, 2019: Tropical cyclones and climate change assessment. Part I: Detection and attribution. *Bull. Amer. Meteor. Soc.*, **100**, 1987–2007, https://doi.org/10.1175/BAMS-D-18-0189.1.

Kobayashi, S., and Coauthors, 2015: The JRA-55 Reanalysis: General specifications and basic characteristics. *J. Meteor. Soc. Japan*, **93**, 5–48, https://doi.org/10.2151/jmsj.2015-001.

Kunkel, K. E., K. Andsager, and D. R. Easterling, 1999: Long-term trends in extreme precipitation events over the conterminous United States and Canada. *J. Climate*, **12**, 2515–2527, https://doi.org/10.1175/1520-0442(1999)012<2515:LTTIEP>2.0.CO;2.

——, D. R. Easterling, D. A. R. Kristovich, B. Gleason, L. Stoecker, and R. Smith, 2010: Recent increases in U.S. heavy precipitation associated with tropical cyclones. *Geophys. Res. Lett.*, **37**, L24706, https://doi.org/10.1029/2010GL045164.

——, ——, ——, ——, ——, and ——, 2012: Meteorological causes of the secular variations in observed extreme precipitation events for the conterminous United States. *J. Hydrometeor.*, **13**, 1131–1141, https://doi.org/10.1175/JHM-D-11-0108.1.

Lin, L., Z. Wang, Y. Xu, and Q. Fu, 2016: Sensitivity of precipitation extremes to radiative forcing of greenhouse gases and aerosols. *Geophys. Res. Lett.*, **43**, 9860–9868, https://doi.org/10.1002/2016GL070869.

Mascioli, N. R., A. M. Fiore, M. Previdi, and G. Correa, 2016: Temperature and precipitation extremes in the United States: Quantifying the responses to anthropogenic aerosols and greenhouse gases. *J. Climate*, **29**, 2689–2701, https://doi.org/10.1175/JCLI-D-15-0478.1.

Massey, N., and Coauthors, 2015: Weather@home—Development and validation of a very large ensemble modeling system for probabilistic event attribution. *Quart. J. Roy. Meteor. Soc.*, **141**, 1528–1545, https://doi.org/10.1002/qj.2455.

Meinshausen, M., and Coauthors, 2011: The RCP greenhouse gas concentrations and their extension from 1765 to 2300. *Climatic Change*, **109**, 213–241, https://doi.org/10.1007/s10584-011-0156-z.

Menne, M. J., I. Durre, R. S. Vose, B. E. Gleason, and T. G. Houston, 2012: An overview of the Global Historical Climatology Network-Daily database. *J. Atmos. Oceanic Technol.*, **29**, 897–910, https://doi.org/10.1175/JTECH-D-11-00103.1.

Min, S.-K., X. Zhang, F. W. Zwiers, and G. C. Hegerl, 2011: Human contribution to more-intense precipitation extremes. *Nature*, **470**, 378–381, https://doi.org/10.1038/nature09763.

Mizuta, R., and Coauthors, 2017: Over 5000 years of ensemble future climate simulations by 60-km global and 20-km regional atmospheric models. *Bull. Amer. Meteor. Soc.*, **98**, 1383–1398, https://doi.org/10.1175/BAMS-D-16-0099.1.

National Academies of Sciences, Engineering, and Medicine, 2016: *Attribution of Extreme Weather Events in the Context of Climate Change*. The National Academies Press, 186 pp., https://doi.org/10.17226/21852.

Neale, R. B., and Coauthors, 2012: Description of the NCAR Community Atmosphere Model (CAM 5.0). NCAR Tech. Note NCAR/TN-486+STR, 274 pp., www.cesm.ucar.edu/models/cesm1.0/cam/docs/description/cam5_desc.pdf.

O'Gorman, P. A., and T. Schneider, 2009: The physical basis for increases in precipitation extremes in simulations of 21st-century climate change. *Proc. Natl. Acad. Sci. USA*, **106**, 14 773–14 777, https://doi.org/10.1073/pnas.0907610106.

Paik, S., S.-K. Min, X. Zhang, M. Donat, A. King, and Q. Sun, 2020: Determining the anthropogenic greenhouse gas contribution

to the observed intensification of extreme precipitation. *Geophys. Res. Lett.*, **47**, e2019GL086875, https://doi.org/10.1029/2019GL086875.

Pall, P., M. R. Allen, and D. A. Stone, 2007: Testing the Clausius–Clapeyron constraint on changes in extreme precipitation under CO_2 warming. *Climate Dyn.*, **28**, 351–363, https://doi.org/10.1007/s00382-006-0180-2.

——, T. Aina, D. A. Stone, P. A. Stott, T. Nozawa, A. G. J. Hilberts, D. Lohmann, and M. R. Allen, 2011: Anthropogenic greenhouse gas contribution to flood risk in England and Wales in autumn 2000. *Nature*, **470**, 382–385, https://doi.org/10.1038/nature09762.

Pfahl, S., P. A. O'Gorman, and E. M. Fischer, 2017: Understanding the regional pattern of projected future changes in extreme precipitation. *Nat. Climate Change*, **7**, 423–427, https://doi.org/10.1038/nclimate3287.

Prein, A. F., C. Liu, K. Ikeda, R. Bullock, R. M. Rasmussen, G. J. Holland, and M. Clark, 2017: Simulating North American mesoscale convective systems with a convection-permitting climate model. *Climate Dyn.*, **55**, 95–110, https://doi.org/10.1007/s00382-017-3993-2.

Risser, M. D., and M. F. Wehner, 2017: Attributable human-induced changes in the likelihood and magnitude of the observed extreme precipitation during Hurricane Harvey. *Geophys. Res. Lett.*, **44**, 12 457–12 464, https://doi.org/10.1002/2017GL075888.

Roeckner, E., and Coauthors, 2003: The atmospheric general circulation model ECHAM5. Part I: Model description. Max Planck Institute for Meteorology Rep. 349, 127 pp.

Shin, S., and P. D. Sardeshmukh, 2010: Critical influence of the pattern of tropical ocean warming on remote climate trends. *Climate Dyn.*, **36**, 1577–1591, https://doi.org/10.1007/s00382-009-0732-3.

Sillmann, J., V. Kharin, F. Zwiers, X. Zhang, and D. Bronaugh, 2013: Climate extremes indices in the CMIP5 multimodel ensemble: Part II. Future climate projections. *J. Geophys. Res. Atmos.*, **118**, 2473–2493, https://doi.org/10.1002/jgrd.50188.

Solomon, A., and M. Newman, 2012: Reconciling disparate twentieth-century Indo-Pacific Ocean temperature trends in the instrumental record. *Nat. Climate Change*, **2**, 691–699, https://doi.org/10.1038/nclimate1591.

Stott, P. A., and Coauthors, 2013: Attribution of weather and climate-related extreme events. *Climate Science for Serving Society: Research, Modelling and Prediction Priorities*, Springer, 307–337.

Sun, L., D. Allured, M. Hoerling, L. Smith, J. Perlwitz, and D. Murray, 2018: Drivers of 2016 record Arctic warmth assessed using climate simulations subjected to factual and counterfactual forcing. *Wea. Climate Extremes*, **19**, 1–9, https://doi.org/10.1016/j.wace.2017.11.001.

Trenberth, K. E., 1999: Conceptual framework for changes of extremes of the hydrological cycle with climate change. *Climatic Change*, **42**, 327–339, https://doi.org/10.1023/A:1005488920935.

USGCRP, 2018: *Impacts, Risks, and Adaptation in the United States.* Vol. II, *Fourth National Climate Assessment*, U.S. Global Change Research Program, 1515 pp., https://doi.org/10.7930/NCA4.2018.

van der Wiel, K., and Coauthors, 2016: The resolution dependence of contiguous U.S. precipitation extremes in response to CO_2 forcing. *J. Climate*, **29**, 7991–8012, https://doi.org/10.1175/JCLI-D-16-0307.1.

van Oldenborgh, G., F. Doblas Reyes, S. Drijfhout, and E. Hawkins, 2013: Reliability of regional climate model trends. *Environ. Res. Lett.*, **8**, 014055, https://doi.org/10.1088/1748-9326/8/1/014055.

——, and Coauthors, 2017: Attribution of extreme rainfall from Hurricane Harvey, August 2017. *Environ. Res. Lett.*, **12**, 124009, https://doi.org/10.1088/1748-9326/aa9ef2.

Wehner, M. F., R. Smith, P. Duffy, and G. Bala, 2010: The effect of horizontal resolution on simulation of very extreme US precipitation events in a global atmosphere model. *Climate Dyn.*, **32**, 241–247, https://doi.org/10.1007/s00382-009-0656-y.

——, and Coauthors, 2014: The effect of horizontal resolution on simulation quality in the Community Atmospheric Model, CAM5.1. *J. Adv. Model. Earth Syst.*, **6**, 980–997, https://doi.org/10.1002/2013MS000276.

Westra, S., L. V. Alexander, and F. W. Zwiers, 2013: Global increasing trends in annual maximum daily precipitation. *J. Climate*, **26**, 3904–3918, https://doi.org/10.1175/JCLI-D-12-00502.1.

Willett, K., A. Simmons, and D. Berry, 2014: Global climate surface humidity [in "State of the Climate in 2013"]. *Bull. Amer. Meteor. Soc.*, **95** (7), S19–S20, https://journals.ametsoc.org/view/journals/bams/95/7/2014bamsstateoftheclimate.1.xml.

Williams, A. P., and Coauthors, 2020: Large contribution from anthropogenic warming to an emerging North America megadrought. *Science*, **368**, 314–318, https://doi.org/10.1126/science.aaz9600.

Wuebbles, D. J., D. W. Fahey, K. A. Hibbard, D. J. Dokken, B. C. Stewart, and T. K. Maycock, Eds., 2017: Climate Science Special Report. Vol. I, *Fourth National Climate Assessment*, U.S. Global Change Research Program Rep., 407 pp., https://doi.org/10.7930/J0J964J6.

Xie, P., M. Chen, S. Yang, A. Yatagai, T. Hayasaka, Y. Fukushima, and C. Liu, 2007: A gauge-based analysis of daily precipitation over East Asia. *J. Hydrometeor.*, **8**, 607–626, https://doi.org/10.1175/JHM583.1.

Ye, H., E. J. Fetzer, S. Wong, A. Behrangi, E. T. Olsen, J. Cohen, B. H. Lambrigtsen, and L. Chen, 2014: Impact of increased water vapor on precipitation efficiency over northern Eurasia. *Geophys. Res. Lett.*, **41**, 2941–2947, https://doi.org/10.1002/2014GL059830.